

Dinuclear vs Tetranuclear $\text{Co}^{\text{II}}\text{Y}^{\text{III}}$ complexes: The effect of increasing molecular size on the relaxation dynamics.

Alberto Masegosa,[⊥], María A. Palacios,[⊥]Eliseo Ruiz[#], Silvia Gómez-Coca, [#] J. Krzystek,[¶] José. M. Moreno,[⊥] Enrique Colacio[⊥]

[⊥]Departamento de Química Inorgánica, Facultad de Ciencias, Universidad de Granada, 18071 Granada, Spain

[#]Departament de Química Inorgànica and Institut de Recerca de Química Teòrica i Computacional, Universitat de Barcelona, Diagonal 645, Barcelona E-08028, Spain

[¶]National High Magnetic Field Laboratory, Florida State University, Tallahassee, Florida 32310, USA

Abstract

A new $\text{Co}^{\text{II}}_2\text{Y}^{\text{III}}_2$ complex with the formula $[\{\text{Co}(\mu\text{-L})\text{Y}(\text{NO}_3)\}_2(\mu\text{-CO}_3)_2]\cdot 2\text{CH}_3\text{OH}\cdot 2\text{H}_2\text{O}$ (where $\text{H}_2\text{L} = \text{N,N',N''-trimethyl-N,N''-bis(2-hydroxy-3-methoxy-5-methylbenzyl)diethylenetriamine}$) has been prepared and its structure solved by single-crystal X-Ray diffraction. The tetranuclear structure is formed by the connection of two $[\text{Co}(\mu\text{-L})\text{Y}(\text{NO}_3)]$ dinuclear units through two carbonate bridging ligands, which exhibit a $\mu_3\text{-}\kappa^2\text{-O,O} : \kappa\text{-O} : \kappa\text{-O}$ tetradentate coordination mode. The Co^{II} ion exhibits a slightly trigonally distorted CoN_3O_3 coordination environment. From direct-current magnetic data a large and positive axial anisotropy parameter was extracted ($D = +82.62 \text{ cm}^{-1}$) and its sign unambiguously confirmed by HFEPR spectra and *ab initio* calculations. The extracted D value is rather larger than those previously reported for the analogous $\text{Co}^{\text{II}}\text{Y}^{\text{III}}$ dinuclear complexes, which agrees with the fact that the Co^{II} ion in the $\text{Co}^{\text{II}}_2\text{Y}^{\text{III}}_2$ complex exhibits the lower distortion from the octahedral geometry in this family of $\text{Co}^{\text{II}}_m\text{Y}^{\text{III}}_m$ complexes. Dynamic *ac* magnetic measurements show that the reported compound presents field-induced slow relaxation for magnetization reversal, through a combination of direct and Raman processes below and above 4 K, respectively. Magnetic measurements on the diluted magnetic counterpart ($\text{Zn}/\text{Co} = 10/1$) show the persistence of these processes, pointing out their single-ion origin. The Raman relaxation process for the Co_2Y_2 complex is faster than those observed for the CoY dinuclear counterparts. This fact and the existence of the persistent direct process at low temperature could be because the former molecule is larger and flexible than the latter ones.

Introduction

Single-Molecule Magnets (SMMs) are an appealing type of molecular magnetic materials based on discrete metal complexes, which are attracting the research attention some thirty years ago.¹ The field of SMMs lies at the boundary between the quantum and classical worlds. Thus, they display classical properties, such as slow relaxation of the magnetization, responsible for magnetic hysteresis (similar to that of bulk magnets) below the so-called blocking temperature (T_B), and quantum properties, such quantum tunnelling of magnetization (QTM), quantum phase interference and quantum coherence.^{1,2} The fascinating physical properties of these nanomagnets make of SMMs promising candidates for potential future applications, among other areas, in ultra-high density magnetic information storage, nanotechnology, molecular spintronics, and as qubits for quantum computing at molecular level.² The SMM behaviour arises from the existence of an energy barrier (U) for the magnetization reversal within the bistable magnetic ground state. This energy barrier permits blocking of the molecular magnetization either parallel or antiparallel to the magnetic field when the polarizing field is removed below T_B , thus leading to slow relaxation of the magnetization. The earlier examples of SMMs were polynuclear metal complexes containing anisotropic transition and lanthanide metal ions, because magnetic anisotropy is an essential requirement for existing U and SMM behaviour.⁴ However, owing to the fact that the anisotropy of the whole molecule is difficult to control in polynuclear metal complexes, low values of the molecular magnetic anisotropy are generally observed, particularly in the case of transition metal clusters.⁵ In view of this, the research in the field focused on mononuclear SMMs (also called Single-Ion magnets, SIMs), which can exhibit larger anisotropy than their polynuclear counterparts. This strategy has been shown to be the most appropriate to achieve SMMs with improved properties. Specifically, some Dy^{III} SIMs exhibit T_B as high as 60 K,⁶ and one of the high temperature SMM is soluble and stable and therefore good candidate for technological applications.⁷

In SIMs based on transition metal ions, the magnitude of D is dictated by the angular momentum, which in turn is modulated by the type of metal ion (coordination number, oxidation state, nature of the ground spin state). Low coordination numbers and oxidation states promote weak ligand fields, which favour large values of the orbital angular momentum and therefore a strong spin-orbit coupling and magnetic anisotropy.⁸ In addition, for integer spin systems an under-barrier tunnelling mechanism occurs, quenching slow relaxation even in the presence of magnetic field, whereas for non-integer spin systems (Kramers ions), in

absence of magnetic field, neither direct phonon-induced nor QTM transitions between the states of the ground doublet can be induced by the modulation of the crystal field (van Vleck cancellation)⁹. Moreover, the lack of fast QTM favours Orbach and Raman thermally activated relaxation processes. In view of the above considerations, the research in this field has focused on mononuclear metal complexes with strong magnetic anisotropy, bearing transition metal ions with significant first order orbital angular momentum.¹⁰ This is presumably the reason why mononuclear complexes containing Co^{II} ($S = 3/2$) with different geometries are by far the most studied SIMs.¹⁰ Although the SIMs behaviour has been observed for Co^{II} complexes with both $D > 0$ and $D < 0$, the former ones are much more numerous (including Co^{II}Y^{III} and mixed valence Co^{II}-Co^{III} complexes). It is worth noting that six-coordinated Co^{II} complexes have been widely studied for SIMs behaviour and the results show that those with $D < 0$ are restricted to a few instances, some of them exhibiting slow magnetization relaxation at zero *dc* field above 2 K. However, it has been recently demonstrated using basic principles that six-coordinated Co^{II} complexes with $D > 0$ (easy-plane anisotropy) can in no case exhibit SIMs behaviour at zero field.⁹ Nevertheless, in the presence of an applied magnetic field, the electronuclear spin states arising from hyperfine interactions steadily acquire a non-zero magnetic moment due to the Zeeman interactions, and slow relaxation of the magnetization can appear. Recently, we have shown for dinuclear Co^{II}Y^{III} complexes (considered as mononuclear SMMs as the Y^{III} ion is diamagnetic), that, even in the presence of a *dc* field, slow magnetization relaxation cannot be observed due to the existence of a persistent fast QTM, which is promoted by intermolecular dipolar interactions.¹¹ By using magnetically diluted Co^{II} complexes prepared by cocrystallization with an isostructural Zn^{II} compound, the intermolecular dipolar interactions and, consequently, the QTM are at least partially suppressed and, in the presence of magnetic field, "hidden SIM" could emerge. As a continuation of this work with Co^{II}Y^{III} complexes, we are interested in analysing how the increase of in size going from a dinuclear Co^{II}Y^{III} to a tetranuclear Co₂Y₂ complex influences the dynamic magnetic properties. With this aim in mind, in this paper we report the synthesis, X-ray structure, HFEPR spectra, detailed (*dc*) and (*ac*) magnetic properties and *ab initio* theoretical calculations of a carbonate-bridged tetranuclear Co₂Y₂ complex with the molecular formula $[\{\text{Co}(\mu\text{-L})\text{Y}(\text{NO}_3)\}_2(\mu\text{-CO}_3)_2] \cdot 2\text{CH}_3\text{OH} \cdot 2\text{H}_2\text{O}$

1 ($\text{H}_2\text{L} = \text{N,N',N''-trimethyl-N,N''-bis(2-hydroxy-3-methoxy-5-methylbenzyl)diethylenetriamine}$). In addition to the role of the size of the complex, we are also interested in investigating how the changes produced by the carbonate-bridging ligand in the distorted octahedral coordination sphere of the Co^{II} ions influence the magnitude of D .

Results and Discussion

Complex **1** has been prepared as pink prismatic-shaped crystals suitable for X-ray analysis from the reaction of H₂L with Co(NO₃)₂·6H₂O and subsequently with Y(NO₃)₃·6H₂O, triethylamine and Na₂CO₃ in MeOH using a 1:1:1:1:2 molar ratio.

Complex **1** crystallizes in the *P2₁/n* space group and is isostructural to the Zn₂Dy₂ complex previously reported by some of us.¹² The centrosymmetric tetranuclear scaffolding of **1** is made of two [Co(μ-L)Y(NO₃)] dinuclear units joined by two carbonate bridging ligands, which exhibit a μ₃-κ₂-O,O : κ-O : κ-O tetradentate coordination mode. The carbonate ligand is coordinated in a chelate mode to the Y₃₊ ion of a Co^{II}Y^{III} dinuclear entity, whereas the third oxygen atom is bonded to the Co₂₊ ion of a centrosymmetrically related dinuclear unit. Moreover, the Y₃₊ ions are bridged by one of the oxygen atoms of the chelating part of each carbonate ligand in a non-symmetric form, generating a rhomboidal Y(O)₂Y bridging unit. Co^{II} and Y^{III} ions of each [Co(μ-L)Y(NO₃)] dinuclear unit are bridged by two phenoxido groups of the L₂- ligand. The Co^{II} ion exhibits a slightly trigonally distorted CoN₃O₃ coordination environment, which is formed by the binding in *fac* positions of three oxygen atoms (one belonging to the carbonate ligand and the other two to the phenoxido bridging groups) and the three amine nitrogen atoms of the ligand. The degree of distortion of the Co^{II} coordination polyhedron with respect to the ideal six-vertex polyhedra was calculated using the continuous shape measure theory and SHAPE software (Table S1).¹³ The results indicate that the CoN₃O₃ coordination sphere can be considered as intermediate between trigonal prismatic and octahedral ideal geometries, but very close to this latter with CshM values of 11.801 and 1.444, respectively (the rest of ideal geometries present much higher CshM values). The Co-O and Co-N distances are in the 2.0706(17)-2.1541(17) and 2.182(2)-2.250(2) Å range, respectively.

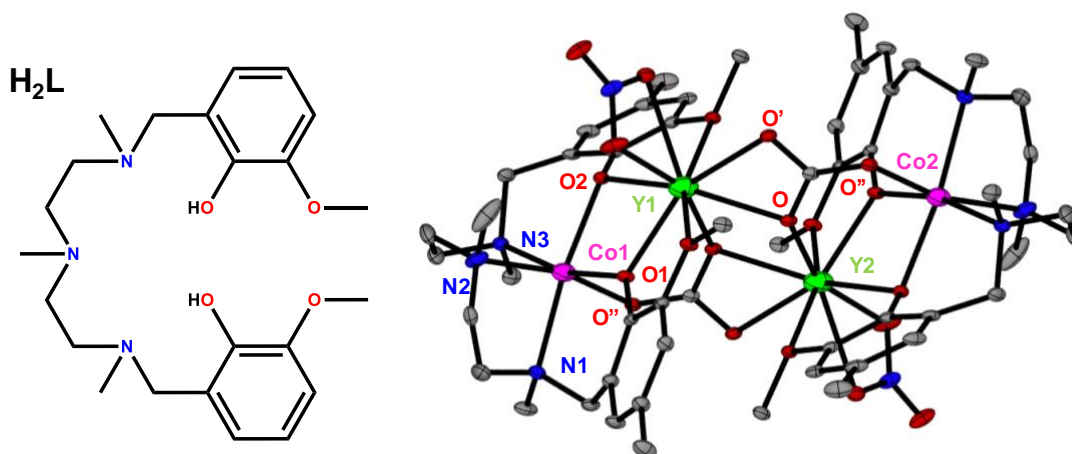


Figure 1. The structure of the ligand H₂L (left) and a perspective view of the structure of **1**. Colour code: N = blue, O = red, Co = pink, Y = green, C = grey. Hydrogen atoms and solvent molecules are omitted for clarity.

The Y₃₊ ion exhibits a somewhat non-symmetrical YO₉ coordination, which is built from the oxygen atoms belonging to the phenoxido bridging groups, the methoxy terminal moieties, the carbonato bridging group and a bidentate nitrate anion. This chelating anion and the chelating part of the carbonato ligand are placed in neighboring positions on the Y₃₊ coordination sphere. The Co...Co, Co...Y and Y...Y distances within the tetranuclear molecule of **1** are 8.278(2), 3.4872(7) and 3.9987(10) Å, respectively. The tetranuclear $\{(\mu_3\text{-CO}_3)_2[\text{Co}(\mu\text{-L})\text{Y}(\text{NO}_3)]_2\}$ molecules are involved in hydrogen bond interactions with the disordered methanol molecule, so that this latter forms hydrogen bonds with one of the oxygen atoms of the chelating part of the carbonato ligand and with the oxygen atom of a water molecule of a neighboring unit, with donor-acceptor distances of 2.628(5) and 2.722(5) Å and 2.799(7) and 2.747(8) Å, respectively. The shortest internuclear Co_{III}...Co_{III} distances are 8.290(2) and 8.4321(15) Å.

Magnetic Properties

The temperature dependence of $\chi_M T$, where χ_M is the molar magnetic susceptibility per tetranuclear Co_{II}Y₂ unit, was measured for complex **1** in the 2-300 K temperature range under an applied magnetic field of 1000 Oe (Figure 2). The $\chi_M T$ value at room temperature of 6.32 cm³mol⁻¹K is larger than that expected (1.875 cm³mol⁻¹K) for an orbitally non-degenerate S = 3/2 ground spin state, which suggests the existence of unquenched orbital contribution of the Co_{II} ion in a distorted octahedral geometry. On lowering temperature, the

$\chi_M T$ product first steadily decreases up to 120 K and then in a sharp manner to reach a value of 4.14 cm³mol⁻¹K at 2 K. This decrease is essentially due to spin-orbit coupling (SOC) effects.

The magnetic susceptibility data for **1** were first analyzed with a model that takes into account the first order SOC effects associated with the $4T_1$ ground term of the octahedral Co^{II} ion, using the T,P isomorphism with an effective orbital moment $L=1$. The corresponding Hamiltonian can be written as:¹⁴

$$\hat{H} = \sigma\lambda\hat{L} \cdot \hat{S} + \Delta\sigma^2[\hat{L}_z^2 - \hat{L}(\hat{L} + 1)/3] + \beta H \cdot (-\sigma\hat{L} + g_i\hat{S}) \quad (\text{equation 1})$$

where λ is the spin-orbit coupling parameter, $\sigma = -A\kappa$ is a combination of the covalency and orbital reduction factor and Δ is the axial orbital splitting of the T_1 term. Using the PHI program,¹⁵ the best-fit was found with the values $\Delta = 199$ cm⁻¹ and $g = 2.22$ with λ and σ fixed to -171 cm⁻¹ and 1.5 , respectively and $R = 3.1 \times 10^{-5}$ ($R = \sqrt{\sum[(\chi_M T)_{\text{exp}} - (\chi_M T)_{\text{calcd.}}]^2 / \sum((\chi_M T)_{\text{exp}})^2}$).

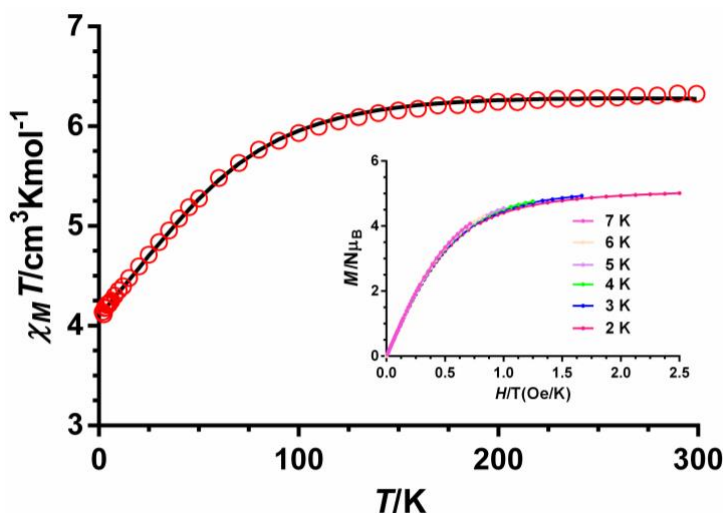


Figure 2.- Temperature dependence of $\chi_M T$ for compound **1**. The solid line represents the best-fit curve using equation 2. M vs H/T plot for compound **1** (inset).

The data were also analysed using a model that takes into consideration the combination of an axial distortion and second-order spin-orbit coupling. As indicated elsewhere, the set of nitrogen and oxygen donor atoms around the Co^{II} ion adopts a *fac* disposition, so that the distorted octahedral CoN_3O_3 coordination polyhedron exhibits an approximate C_{3v} local symmetry. In such a symmetry, the triplet $4T_{1g}$ ground state for the hypothetical ideal O_h symmetry splits into an orbital singlet $4A_2$ and an orbital doublet $4E$. The energy gap between them is described by the axial splitting parameter, Δ . The $4A_2$ and $4E$ levels can undergo an additional split by second order spin-orbit coupling generating two and four Kramers doublets, respectively.^{11a} When Δ is large enough and positive only the two lowest Kramers doublets arising from the $4A_2$ ground term, Γ_6 and Γ_7 , are thermally populated and the energy

gap between them can be envisaged as a zero-field splitting (ZFS) within the quartet state. If so, the following Hamiltonian can be used to analyse the magnetic properties

$$H = D[S_z^2 - S(S + 1)/3] + E(S_x^2 - S_y^2) + g\mu_B H S \text{ (equation 2)}$$

where S is the spin ground state, D and E are the axial and transverse magnetic anisotropies, respectively, μ_B is the Bohr magneton and H the applied magnetic field. If $E = 0$, then $2D$ represents the energy gap between $\pm 1/2$ and $\pm 3/2$ Kramers doublets (KD) arising from second order SOC of the quartet ground state. If $D > 0$, the doublet with $M_s = \pm 1/2$ is at lower energy than the doublet with $M_s = \pm 3/2$, whereas when $D < 0$ the reverse distribution of these doublets occurs. The temperature dependence of the magnetic susceptibility **1** was fitted with the above Hamiltonian using the PHI program (Figure 2).¹⁵ The best fit of the data using an axial g tensor led to the following magnetic parameters: $D = +82.62 \text{ cm}^{-1}$, $E = 0.84 \text{ cm}^{-1}$, $g_{xy} = 2.77$ and $g_z = 2.03$ with $R = 3.9 \times 10^{-6}$ ($R = \sum[(\chi_{MT})_{\text{exp.}} - (\chi_{MT})_{\text{calcd.}}]^2 / \sum((\chi_{MT})_{\text{exp.}})^2$). A very good fit was also obtained for a negative D value affording the following parameters: $D = -67.21 \text{ cm}^{-1}$, $E = 0.74 \text{ cm}^{-1}$, $g_{xy} = 2.69$ and $g_z = 2.54$ with $R = 7.2 \times 10^{-7}$. Therefore, the sign of D cannot be unambiguously determined from powder magnetic susceptibility measurements. It should be noted that the ZFS model (equation 2) reproduces the experimental data better than the first order SO model (equation 1). Therefore, the ZFS model appears to be the most appropriate for interpreting magnetic data. It is worth mentioning at this point that the temperature dependence of the magnetization at different magnetic fields cannot be used to accurately extract the ZFS parameters, because when the ZFS is very large, as in the case of **1**, the M vs H/T isotherms depend only slightly on temperature (see Figure 2 inset).

In order to unequivocally determine the sign of D , we have carried out low-temperature (down to 5 K) high-frequency and -field EPR (HF-EPR) measurements in the 50–650 GHz, and 0–14.5 Tesla range, respectively, on a powder sample of **1** (Figure 3). The observed resonances cannot be due to transitions between the $m_s = \pm 1/2$ and $\pm 3/2$ KDs because the energy gap δ between these KDs is considerably larger than the highest available energy of the sub-THz wave quantum (23 cm^{-1}). If D were negative, the lower-lying KD would be $m_s = \pm 3/2$ and then the transition within this manifold would be nominally forbidden ($\Delta m_s = \pm 3$). In such a case, the EPR spectrum is usually silent if $E/D \sim 0$. Therefore, the HF-EPR spectra can only arise from transitions within the $m_s = \pm 1/2$ manifold, which is allowed because $\Delta m_s = \pm 1$. These facts confirm that the $m_s = \pm 1/2$ KD lies lower in energy than the $m_s =$

$\pm 3/2$ KD and therefore D is positive (Figure 3). In fact the spectra can be well simulated with $D > 0$ under assumption of an axial g -tensor (Figure 3). Although the magnitude of the ZFS cannot be extracted from the transitions within the $m_s = \pm 1/2$ manifold, however, they allow to calculate the E/D rhombicity factor. It is worth mentioning that the g and $|E/D|$ values are not far from those extracted from the fitting of the susceptibility magnetic data (see above).

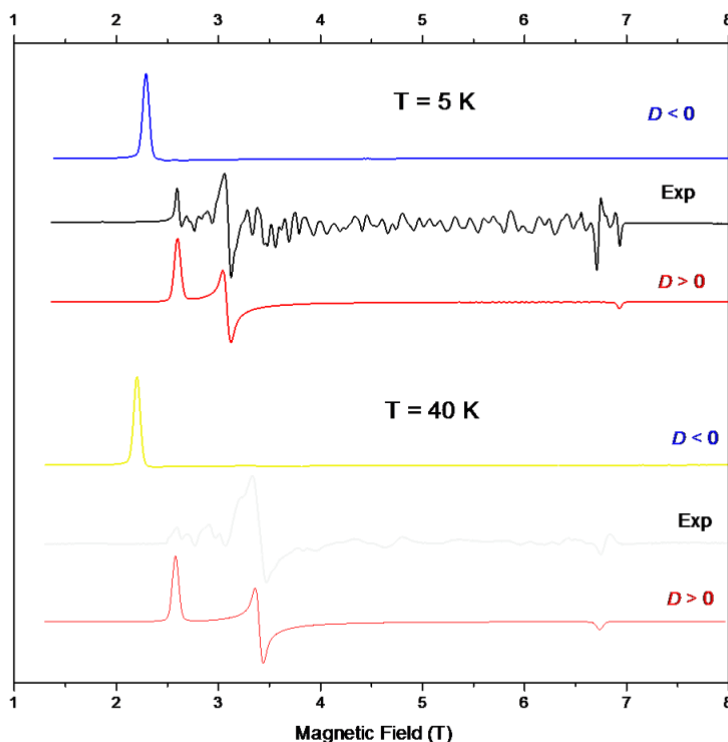


Figure 3. A 101.6 GHz spectra of **1** at 5 and 40 K (black trace) accompanied by two simulations using the following parameters: $|E/D| = 0.059$, $g_{\perp} = 2.58$, $g_{\parallel} = 2.12$ (5 K) and $|E/D| = 0.040$, $g_{\perp} = 2.48$, $g_{\parallel} = 2.24$ (40 K). Red trace: $D > 0$; blue trace: $D < 0$. In each case, $|D|$ was fixed at 80 cm^{-1} (the value obtained by CASSCF + RASSI calculations) and the rhombicity of the zfs tensor was calculated under assumption of an axial g -tensor (i.e. ignoring the rhombicity of g -tensor).

The D positive value extracted from magnetic data is rather larger than those previously reported for the analogous dinuclear complexes $[\text{Co}(\mu\text{-L})(\mu\text{-X})(\text{NO}_3)_2]$ ($\text{X} = \text{acetate}$, benzoate , $9\text{-anthracene carboxylate}$).¹¹ In view of the above results, the magnitude of the ZFS (the energy separation, δ , between the $m_s = \pm 1/2$ and $m_s = \pm 3/2$ Kramers doublets), which is given by $\delta = 2(D_2 + 3E_2)^{1/2}$ is 169.47 cm^{-1} for **1**.

With the aim of underpinning the sign and magnitude of the ZFS for **1**, we have carried out electronic structure CASSCF calculations of the ZFS parameters D and E on the X-ray structure of this complex using MOLCAS software package.¹⁶ The SO-RASSI approach

included in MOLCAS gives rise to following ZFS parameters: $D = +80.00 \text{ cm}^{-1}$, $E = +19.43 \text{ cm}^{-1}$ and $\delta = 173.56 \text{ cm}^{-1}$. Noteworthy, the computed D value is almost coincident in sign and magnitude with that extracted experimentally from magnetic data.

We have previously reported the existence of a non-linear correlation between the *ab initio* calculated D values for the closely related $[\text{Co}(\mu\text{-L})(\mu\text{-X})\text{Y}(\text{NO}_3)_2]$ dinuclear complexes ($X = \text{acetate, benzoate, 9-anthracene carboxylate}$), that only differ in the ancillary bridging ligand.^{11b} For these complexes, the D value decreases with the increase of the distortion from the octahedral geometry quantified by the shape measures parameter (S). The Co_{II} ions in **1** are well separated in the structure ($> 8 \text{ \AA}$), so that dipolar and magnetic interactions, if exist, can be considered as negligible. Therefore, from the magnetic point of view, complex **1** can be considered as two non-interacting $\text{Co}_{\text{II}}\text{Y}_{\text{III}}$ isolated dinuclear units analogous to that of the $[\text{Co}(\mu\text{-L})(\mu\text{-X})\text{Y}(\text{NO}_3)_2]$ complexes and therefore should obey the above indicated magneto-structural correlation. In fact, complex **1** exhibiting the lower S value (1.44) shows the higher D value (see Figure 4).

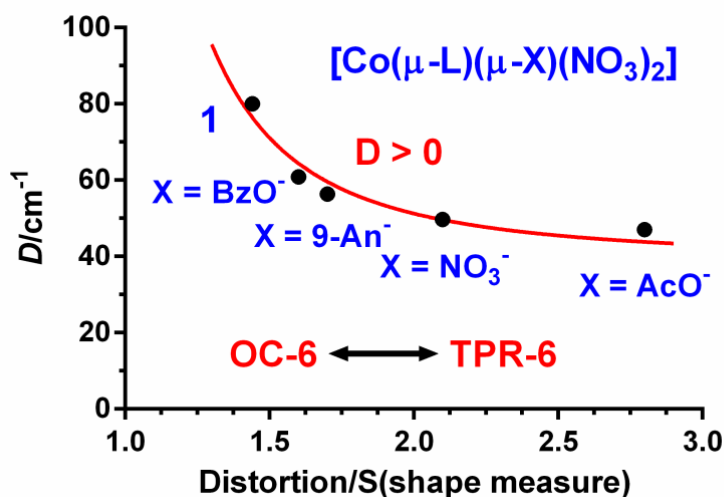


Figure 4.- Correlation between D and the distortion from the octahedral geometry quantified by the shape measures parameter (S).

In order to know if complex **1** shows slow magnetization relaxation and to compare the results with those for the $[\text{Co}(\mu\text{-L})(\mu\text{-X})\text{Y}(\text{NO}_3)_2]$ dinuclear complexes, dynamic *ac* magnetic susceptibility measurements were performed under a 3.5 Oe alternating field. Complex **1** does not show any out-of-phase signals (χ''_{M}) above 2 K at zero applied dc field. This fact is not surprising because, as it has been recently shown for Kramers ions like $\text{Co}(\text{II})$ with $D > 0$, the electronuclear spin states arising from the hyperfine interactions have

negligible magnetic moments at zero field, so that slow relaxation cannot be observed. However, in the presence of an applied dc field, the electronuclear spin states acquire magnetic moment and, if the compound behave as a SMM, slow relaxation could be observed.⁹ It has been recently shown that, even in these conditions, some compounds do not exhibit slow relaxation because the transversal magnetic field created by intermolecular interactions could split the Kramers doublet states opening relaxation pathways for direct and QTM processes.^{11a} In these cases, to observe magnetization relaxation, magnetic dilution with an isostructural diamagnetic counterpart to partly or fully suppress intermolecular interactions, is required.

To analyze the dynamic behavior of **1**, the field dependence of the *ac* magnetic susceptibility measurements at T= 2 K, for magnetic fields varying between 0.025 and 0.25 T, were undertaken. The aim was not only to know if compound **1** exhibits field induced slow magnetization relaxation, but also to investigate how it evolves with the applied magnetic field. After application of a dc magnetic field, compound **1** shows strong frequency dependent out-of-phase signals below 10 K. Nevertheless, none of them exhibit clear maxima above 2 K in the 1-1500 Hz frequency range. It is worth mentioning that two relaxation processes can be observed for $H_{dc} > 0.1$ T, whereas below 0.05 T almost only the fast relaxation process (FR) is operative. We have extracted the relaxation times at different fields for the fast relaxation process (Figure 5) by fitting the frequency dependence of the out-of-phase signal to the Debye model (the field dependence of the relaxation times for the slow process could not be obtained). As it can be observed in Figure 5, $1/\tau$ increases with the increase of the field following a $1/\tau$ vs H^4 law, which is typical of a direct process. Therefore, it seems that, at low temperature, **1** does not show QTM but a direct relaxation process. It should be pointed out that experimental and theoretical studies have shown that the Orbach relaxation process can be generally ruled out for easy-plane anisotropic Co^{II} complexes with SIM behavior.^{11b} Therefore, above about 4 K almost only the Raman spin-phonon relaxation contributes to the FR process.

The slow process (induced by magnetic fields larger than 0.1 T) is rather usual in SMMs that are subjected to a magnetic field, and it is generally due to a spin-phonon direct relaxation process promoted by the split of the Kramers degeneration when a magnetic field is applied (the larger is the energy gap between the two m_s ground states, the higher is the phonon density with an energy equal to this gap).¹⁷

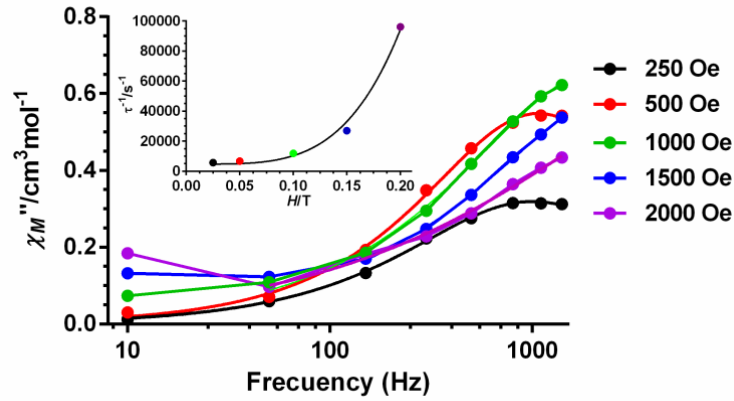


Figure 5.- Field dependence of the out-of-phase signal (χ''_M) at 2 K. Inset: Field dependence of the relaxation times at 2 K..

In view of the above field dependence of the relaxation times for the FR process, temperature and frequency ac measurements were carried out under a static field of 0.025 T. The strong intensity of the signals corresponding to the direct process at low temperature modulates the intensity of the signals due to Raman relaxation at higher temperatures, so that no clear maxima are observed and only an incipient shoulder appears above 4 K in the temperature dependence of the χ''_M plots at different frequencies (Figure S2). The ac data for the FR process could not be correctly fitted to the Debye model because the FR peaks lie above the studied frequency range (Figure S1). Nevertheless, we have used an alternative approach to extract the relaxation parameters from the ac data. The ratio between the out-of-phase and in phase ac susceptibility can be expressed in an approximate manner as $\chi''_M/\chi'_M = 2\pi f\tau$ (equation 3). The replacement in this equation of the relaxation time (τ) by its expression for each relaxation mechanism would allow extracting the corresponding relaxation parameters. If we assume that hypothetically the relaxation takes place exclusively through an Orbach relaxation mechanism, for which $\tau = \tau_0 \exp(-U_{eff}/k_B T)$, the following equation would become:

$$\ln(\chi''_M/\chi'_M) = \ln(2\pi f\tau_0) - U_{eff}/k_B T \text{ (equation 4)}$$

The energy barrier could be approximately estimated by fitting of the experimental χ''/χ' data in the high frequency region to equation 4. The best fit at different frequencies (Figure 6) leads to the following parameters: $U_{eff}/k_B \approx 7.9$ K and $\tau_0 \approx 4.6 \times 10^{-6}$ s. The extracted U_{eff} value is much lower than the experimental energy gap between the ground $S = \pm 1/2$ and the excited state $S = \pm 3/2$ extracted from static susceptibility measurements. This result once again

confirms, as indicated above, that the magnetization reversal for field induced CoII SIMs with $D > 0$ does not take place through an Orbach process but through direct and Raman processes, which predominate at low at high temperatures, respectively.

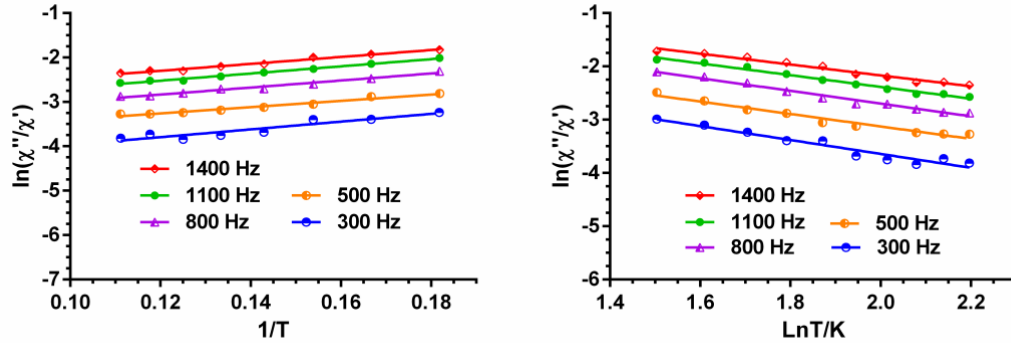


Figure 6.- Temperature dependence of the ratio of the in-phase and out-of-phase ac components at different frequencies under a magnetic field of 0.025 T. Solid lines correspond to the fit of the experimental data to equation 4 (left) and equation 5 (right).

In view of the fact that at high temperatures the relaxation must proceed through a Raman process, we have fitted the χ''/χ' data to the following equation:

$$\ln(\chi''_M/\chi'_M) = \ln(2\pi fC) - n(\ln T) \quad (\text{equation 5})$$

where in equation 3, τ has been replaced by the power law $\tau_{-1} = CT^n$. The data in the 5.5 - 9.5 K range were fitted to the equation 5 using frequencies between 300 and 1400 Hz. The fitting procedure led to the following parameters: $C = 0.00014 \text{ s}^{-1}\text{K}^n$ and $n = 1.16$. Although $n = 9$ for Kramers ions,¹⁸ however, if both, acoustic and optical phonons, are taken into account, n values between 1 and 6 can be considered as acceptable.¹⁹ Therefore, it is clear that the Raman process dominates at high temperature and low fields for the FR process.

In order to know how the dynamic relaxation parameters evolve with the magnetic field, we have taken ac susceptibility measurements under a static magnetic field of 0.25 T (Figures S3-S5). It is of interest that the overall dynamic behavior is similar to that observed under 0.025 T, but the relaxation parameters change to the following values: $U_{\text{eff}}/k_B \approx 17.2 \text{ K}$ and $\tau_0 \approx 6.6 \times 10^{-7} \text{ s}$ using equation 4 and $C = 0.005 \text{ s}^{-1}\text{K}^n$ and $n = 2.18$ for equation 5. In view of these results, it appears that the Raman process slows down by increasing the static magnetic field.

Compared to the analogous $\text{Co}_{\text{II}}\text{Y}_{\text{III}}$ dinuclear complexes $[\text{Co}(\mu\text{-L})(\mu\text{-X})\text{Y}(\text{NO}_3)_2]$ ($\text{X} = \text{nitrate, benzoate, acetate, 9-anthracenecarboxylato}$),¹¹ the dynamic behaviour of **1** is quite different. Thus, the dinuclear complexes $[\text{Co}(\mu\text{-L})(\mu\text{-X})\text{Y}(\text{NO}_3)_2]$ ($\text{X} = \text{nitrate and acetate}$) exhibit fast QTM, which is almost suppressed in the presence of a field of 0.1 T, so that clear maxima appear in the temperature and frequency dependence of the out-of-phase component of the ac susceptibility in the 2–6 K temperature range. On the other hand, the complexes $[\text{Co}(\mu\text{-L})(\mu\text{-X})\text{Y}(\text{NO}_3)_2]$ ($\text{X} = \text{benzoate and 9-anthracenecarboxylato}$)^{11b,c} do not show any out-of-phase signal even in the presence of magnetic field and need to be magnetically diluted to suppress intermolecular interactions and to observe slow relaxation.^{11b,c} This is due to the existence of strong intermolecular interactions that favour the fast QTM. The dilution process suppresses intermolecular interactions and then field-induced neat maxima are also observed in the 2–6 K range in the $\chi''_{\text{MVS}} T$ plot at different frequencies. In spite of the absence of significant intermolecular interactions in **1** ($\text{Co}\cdots\text{Co}$ distance is larger than 8.0 Å and there are no $\pi\cdots\pi$ interactions), and in contrast to the $\text{Co}_{\text{II}}\text{Y}_{\text{III}}$ dinuclear complexes $[\text{Co}(\mu\text{-L})(\mu\text{-X})\text{Y}(\text{NO}_3)_2]$ ($\text{X} = \text{nitrate and acetate}$), the temperature and frequency dependence of χ''_{M} of **1** does not show any neat maximum after applying magnetic fields up to 0.25 T, either in diluted or pristine forms. Instead, as indicated elsewhere, a strong signal appears at very low temperature (below 4 K), which does not arise from QTM but from a spin-phonon direct process.

It should be pointed out that, sometimes, the application of a magnetic field on octahedral Co_{II} complexes promotes the emergence of two well-differentiate relaxation processes, one of them originated from dipolar intermolecular interactions.²⁰ Interestingly, this latter relaxation process disappears in some cases with the increase of the magnetic field and in other cases when the magnetic field decreases. As expected, this relaxation process due to intermolecular dipolar interactions disappears in the magnetic diluted complexes. However, the magnetic diluted complex **1'** (with a $\text{Zn/Co} = 10/1$ magnetic site dilution) shows a similar behaviour to **1** (Figure S6), pointing out the single-ion origin of the magnetic relaxation. Owing to the poor signal to noise ratio, a detailed analysis of the relaxation dynamics of **1'** is not feasible.

It has recently shown, from experimental and theoretical results, that the temperature dependence of the spin relaxation depends on the electronic structure as well as the vibrational characteristics of the specific SMM.²¹ Therefore, the frequency and lifetime of phonons together with spin-phonon coupling coefficients strongly affect the relaxation time. In this regard, internal vibrations play an essential role in connecting the spin states and

phonons that contribute to the spin-relaxation pathways. Nevertheless, only a few local vibrational modes with the lowest frequency are active at low temperature. The reduction of the molecular size should favour the decreasing of the relaxation rate because there will be less degrees of freedom that can combine with the local vibrations.²² Moreover, it has been suggested that the direct relaxation between two quasi-degenerate ground states is accelerated in structurally flexible SMMs.²¹ In view of the above considerations, it is not unexpected that the tetranuclear $\text{Co}_{\text{II}}\text{Y}_{\text{III}}\text{2}$ compound, which is larger and flexible than the dinuclear $\text{Co}_{\text{II}}\text{Y}_{\text{III}}$ counterparts, exhibits a persistent and intense direct relaxation process at low temperature. Nevertheless, more examples of similar compounds with different size and flexibility are needed to support this hypothesis.

Conclusions

The compartmental ligand N,N',N'' -trimethyl- N,N' -bis(2-hydroxy-3-methoxy-5-methylbenzyl)diethylenetriamine has been successfully used to prepare a new $\text{Co}_{\text{II}}\text{Y}_{\text{III}}\text{2}$ complex. In this compound, the centrosymmetric $\text{Co}_{\text{II}}\text{Y}_{\text{III}}\text{2}$ tetranuclear entity is made of two $[\text{Co}(\mu\text{-L})\text{Y}(\text{NO}_3)]$ dinuclear units connected by two carbonate bridging ligands with $\kappa\text{-O,O':}\kappa\text{-O:}\kappa\text{O''}$ tetradentate coordination mode. The *ab initio* calculated axial anisotropy parameter (D) in this family of dinuclear and tetranuclear $\text{Co}_{\text{II}_n}\text{Y}_{\text{III}_n}$ complexes correlates with the distortion of the CoN_3O_3 coordination polyhedron from the ideal octahedral geometry to trigonal prismatic, so that D decreases with increasing the distortion from octahedral geometry. Among the $\text{Co}_{\text{II}_n}\text{Y}_{\text{III}_n}$ complexes, the reported $\text{Co}_{\text{II}}\text{Y}_{\text{III}}\text{2}$ compound exhibits the lower distortion from an octahedral geometry and therefore the larger anisotropy ($D = +82.62 \text{ cm}^{-1}$). This complex shows two relaxation processes for $H_{\text{dc}} > 0.1 \text{ T}$, whereas below 0.05 T almost only the fast relaxation process (FR) is operative. Below 4 K and under a static field of 0.025 T the $\text{Co}_{\text{II}}\text{Y}_{\text{III}}\text{2}$ complex does not show QTM but a direct relaxation process, whereas above 4 K the Raman spin-phonon relaxation process is dominant.

As expected, there is no correlation between D value and the magnetization dynamics for this family of $\text{Co}_{\text{II}_n}\text{Y}_{\text{III}_n}$ complexes, thus confirming that the magnetization reversal takes place through relaxation processes others than the Orbach one. The fact that the Raman relaxation process for the $\text{Co}_{\text{II}}\text{Y}_{\text{III}}\text{2}$ complex is faster than those observed for the $\text{Co}_{\text{II}}\text{Y}_{\text{III}}$ dinuclear counterparts, as well as the persistence of the direct process at low temperature under different static magnetic fields and after magnetic dilution, could presumably be a consequence to the larger size and flexibility of the former molecule with respect to the latter ones.

Experimental

Synthetic procedures

General Procedures: Unless stated otherwise, all reactions were conducted in oven-dried glassware in aerobic conditions, with the reagents purchased commercially and used without further purification. The H₂L ligand was prepared as previously reported.²³

Synthesis of $[\{Co(\mu-L)Y(NO_3)_2(\mu-CO_3)_2\} \cdot 2CH_3OH \cdot 2H_2O(1)$: To a solution of the ligand (0.056 g, 0.125 mmol) in methanol (15 ml) was subsequently added with continuous stirring Co(NO₃)₂·6H₂O (0.036 g, 0.125 mmol), Y(NO₃)₃·6H₂O (0.048 g, 0.125 mmol) and triethylamine (0.025g, 0.25 mmol). Then, a solution of Na₂CO₃ (0.026 g, 0.25 mmol) in the minimum quantity of water was added dropwise and stirred for 5 minutes. The brown-pink solution was filtered to eliminate any amount of insoluble material and allowed to stand at room temperature. After three days, pink crystals suitable for X-ray diffraction were obtained. Yield: 47 %. Anal. Found: C, 42.86; H, 5.10; N, 7.42. Anal. Calc. for C₅₄H₈₂N₈O₂₄Co₂Y₂: C, 42.59; H, 5.43; N, 7.36. IR (cm⁻¹): 3018, ν(CH)_{aromatic}; 2969(w), 2965(w), 2839(w) ν(CH); 1548 (s), 1345 (s) ν(CO)_{carbonate}.

Syntheses of the diluted sample 1'. This compound was prepared following the same method as for **1**, but using a 1:10 Co/Zn ratio, that is 3.63 mg (0.0125 mmol) of Co(NO₃)₂·6H₂O and 33.46 mg (0.1125 mmol) of Zn(NO₃)₂·6H₂O. From the resulting solution a pale pink microcrystalline precipitated. The X-ray powder spectrum demonstrates that this compound is isostructural with the undiluted complex (see Figure S7).

Physical measurements

Elemental analyses were performed at the “Centro de Instrumentacion Cientifica” (University of Granada) on a Fisons-Carlo Erba analyser model EA 1108. IR spectra on powdered samples were recorded with a Thermo Nicolet IR200FTIR using KBr pellets.

Variable-temperature (2–300 K) magnetic susceptibility measurements on polycrystalline samples of **1** and **1'** under an applied field of 1000 Oe were carried out with a Quantum Design SQUID MPMS XL-5 device. Alternating-current (ac) susceptibility measurements under different applied static fields were performed using an oscillating ac field of 3.5 Oe and ac frequencies ranging from 1 to 1500 Hz. The experimental susceptibilities were corrected for

the sample holder and diamagnetism of the constituent atoms using Pascal's tables. A pellet of the sample cut into very small pieces was placed in the sample holder to prevent any torquing of the microcrystals.

HFEPR measurements were performed at the NHMFL at several subterahertz frequencies between 50 and 650 GHz and low temperatures on loose powders and pellets, using an instrument described previously in detail²⁴ with the exception of a Virginia Diodes subterahertz wave source, consisting of a 13 ± 1 GHz frequency generator and a cascade of amplifiers and frequency multipliers.

The X-ray powder diffraction (XRPD) spectra were registered on a (2 θ) Bruker D2-PHASE using $\text{CuK}\alpha$ ($\lambda = 1.5418 \text{ \AA}$) radiation and LINXEYE detector, from 5 to 50 ° (2 θ) at a scanning rate of 0.5 ° 2 θ /min.

Single-Crystal Structure Determinations.

Suitable crystals of **1** were mounted on a glass fibre and used for data collection. X-ray diffraction data of **1** were collected at 110 K using a Bruker AXS SMART APEX CCD diffractometer ($\text{MoK}\alpha$ radiation, $\lambda = 0.71073 \text{ \AA}$) outfitted with a CCD area-detector and equipped with an Oxford Cryosystems 700 series Cryostream device. Unit-cell parameters were determined and refined on all observed reflections using APEX2 software.²⁵ Correction for Lorentz polarization and absorption were applied by SAINT and SADABS programs, respectively.^{26,27}

The structures were solved by direct methods and refined by the full-matrix least-squares method on F^2 using the SHELX software suite and SHELXL-2014 program.²⁸ All non-hydrogen atoms were refined anisotropically. Hydrogen atom positions were calculated and isotropically refined as riding models to their parent atoms. A summary of selected data collection and refinement parameters can be found from the Supporting Information (Table S1) and [CCDC 1544559](#).

Computational methodology

The calculation of zero-field splitting parameters (D and E) were carried out with the MOLCAS₁₆ software package. We have used MOLCAS (along with the SINGLE_ANISO²⁹ code) to carry out CASSCF calculations of the energy states of the $\text{Co}_{2\text{II}}\text{Y}_{2\text{III}}$ complexes. Then, spin-orbit coupling has been considered, as implemented in the SO-RASSI (Restricted Active Space State Interaction) approach, to mix up these energies and obtaining the final energy states. In these calculations we have employed an all electron ANO-RCC basis set:³⁰ Co atoms (6s5p4d2f), N (4s3p2d1f), C (3s2p) and H (2s). The active space includes seven electrons in five 3d-orbitals of Co(II) CAS (7,5). We have included all 10 states for the $2S+1=$

4 (quartet) states arising from the $4F$ and $4P$ terms of $Co(II)$, and all the 40 states for the respective $2S+1=2$ (duplet) states arising from the $2P$, $2D$ (twice), $2F$, $2G$ and $2H$ terms of the $Co(II)$ ion.

Acknowledgements

Financial support from Ministerio de Economía y Competitividad (MINECO) for Projects CTQ2014-56312-P and CTQ2015-64579-C3-1-P, the Junta de Andalucía (FQM-195 and the Project of excellence P11-FQM-7756), the University of Granada. M.A. P. thanks to MINECO for a Juan de la Cierva Incorporation contract (IJCI-2014-19485).

References

- 1.-(a) D. Gatteschi; R. Sessoli, *Angew. Chem. Int. Ed. Engl.* **2003**, 42, 268-297. (b) *Molecular Nanomagnets* D. Gatteschi; R. Sessoli, R.; J. Villain; Oxford University Press, Oxford, **2006**. (c) *Molecular Magnets: Physics and Applications*, Ed. J. Bartolomé; F. Luis, F.; J. F. Fernández, Springer-Verlag, Berlin-Heidelberg, **2014**. (d) *Molecular Nanomagnets and Related Phenomena*, Ed. S. Gao, S; *Structure and Bonding*, Springer-Verlag, Berlin-Heidelberg, vol. 164, **2015**.
- 2.-(a) M. N. Leuenberger and D. Loss, *Nature*, **2001**, 410, 789; (b) A. R. Rocha, V. M. García-Suárez, S. W. Bailey, C. J. Lambert, J. Ferrer, S. Sanvito, *Nat. Mater.*, **2005**, 4, 335-9; (c) A. Ardavan, O. Rival, J. L. Morton, S. J. Blundell, A. M. Tyryshkin, G. A. Timco and R. E. P. Winpenny, *Phys. Rev. Lett.*, **2007**, 98, 057201; (d) L. Bogani and W. Wernsdorfer, *Nat. Mater.*, **2008**, 7, 179; (e) E. Coronado, A. Epstein Eds. *Molecular spintronics and quantum computing*, Themed issue *Journal of Materials Chemistry* **2009**, 12, 1661-1768; (f) M. J. Martínez-Pérez, S. Cardona-Serra, C. Schlegel, F. Moro, P. J. Alonso, H. Prima-García, J. M. Clemente-Juan, M. Evangelisti, A. Gaita-Ariño, J. Sesé, J. Van Slageren, E. Coronado and F. Luis, *Phys. Rev. Lett.*, **2012**, 108, 247213. (g) G. Aromí, D. Aguilà, P. Gamez, F. Luis, O.

Roubeau, *Chem. Soc. Rev.*, **2012**,41, 537-546; (h) R. Vincent, S. Klyatskaya, M. Ruben, W. Wernsdorfer and F. Balestro, *Nature*, **2012**, 488, 357; (i) M. Ganzhorn, S. Klyatskaya, M. Ruben and W. Wernsdorfer, *Nat. Nanotechnol.*, **2013**, 8, 165-169; (j) M. Jenkins, T. Hümmer, M. J. Marínez-Pérez, J. García-Ripoll, D. Zueco and F. Luis, *New J. Phys.*, **2013**, 15, 095007; (k) Molecular Spintronics : The role of Coordination Chemistry, E. Coronado, M. Yamashita, Eds. Themed issue *Dalton Trans.*, **2016**,45, 16553-16584. (l)J. Escalera-Moreno, J. Baldoví A. Gaita-Ariño, E. Coronado, *Chem Sci.***2018**,13, 3265-3275. (m) M. Atzori , S. Benci , E. Morra, L. Tesi, M. Chiesa, R. Torre, L. Sorace, R. Sessoli, *Inorg Chem.* **2018**57, 731-740. (n) Tesi L, Lucaccini E, Cimatti I, Perfetti M, Mannini M, Atzori M, Morra E, Chiesa M, Caneschi A, Sorace L, R. Sessoli, *Chem Sci.***2016**, 7, 2074-2083.

3.-G. Aromi and E. K. Brechin, in *Single-Molecule Magnets and Related Phenomena*, ed. R. Winpenny, **2006**, pp. 1–67

4.- a) F. Neese, F.;D. A. Pantazis, D. A. *Faraday Discuss.*, **2011**, 148, 229-238; b) O. Waldmann, *Inorg. Chem.* 2007, 46, 10035-10037.

5.- (a) O. Waldmann, A.M. Ako, H.U. Gudel, A.K. *Inorg. Chem.* **2008**, 47, 3486–3488. (b) A.J., Tasiopoulos, Vinslava; W., Wernsdorfer;K.A.Abboud, G. Christou,*Angew. Chem. Int. Ed.***2004**,43, 2117–2121.

6.- a) C. A. P. Goodwin, F. Ortu, D. Reta, N. F. Chilton, D. P. Mills, *Nature***2017**, 548, 439; b) F.-S. Guo, B. M. Day, Y.-C. Chen, M.-L. Tong, A. Mansikkamäki, R. A. Layfield, *Angew. Chemie Int. Ed.***2017**, 56, 11445.

7.- L. Norel L. E. Darago, B. Le Guennic, K. Chakarawet, M. I. Gonzalez, J. H. Olshansky, S. Rigaut , J. R. Long, *Angew. Chemie Int. Ed.*, 2018, 57, 1933-1938.

8.- S. Gómez-Coca; E. Cremades; N. Aliaga-Alcalde.; E. Ruiz., *J. Am. Chem. Soc.***2013**, 135, 7010–7018.

- 9.- S. Gómez-Coca; A. Urtizberea; E. Cremades; P. J. Alonso; A. Camón.;E. Ruiz; F. Luis, *Nat. Commun.* **2014**, 5,4300.
- 10.- (a) G. A.Craig,; M. Murrie, *Chem. Soc. Rev.* **2015**, 44, 2135–2147 7. (b) A. K.Bar, C. Pichon, J.-P. Sutter, *Coord. Chem. Rev.* **2016**, 308, 346–380. (c) S. Gómez-Coca, D. Aravena,, R.Morales,E. Ruiz, E.,*Coord. Chem.Rev.***2015**, 289-290, 379–392.(d) J. MFrost,; K. L. M. Harriman,.; Murugesu, M.; *Chem. Sci.* **2016**, 7, 2470– 2491.e) M. Feng, M- LTong, *Chemistry*. 2018,24,7574-7594, f) D. Maniaki,E. Pilichos, S. P. Perlepes, *Front Chem.* **2018** Oct 9;6:461. doi: 10.3389/fchem.2018.00461.
- 11.- (a) E. Colacio, J. Ruiz, E. Ruiz, E. Cremades, J. Krzystek, S. Carretta,J. Cano, T. Guidi, W. Wernsdorfer, E. K Brechin, *Angew. Chem., Int. Ed.* **2013**, 52, 9130–9134. (b) M. A. Palacios, J. Nehr Korn, E.A. Sutura, E. Ruiz, S. Gómez-Coca, K. Holldack, A. Schnegg, J. Krzystek , J. M Moreno, E. Colacio, *Chemistry*, **2017**, 23, 11649-11661. (c) Colacio E. (2018) Mannich Base Ligands as Versatile Platforms for SMMs. In: . *Topics in Organometallic Chemistry*. Springer, Berlin, Heidelberg.
- 12.- S. Titos-Padilla, J. Ruiz, J. M. Herrera, E. K. Brechin, W. Wersndorfer, F. Lloret, E. Colacio, *Inorg Chem.***2013**, 52, 9620-9626.
- 13.-F. Lloret, M. Julve, J. Cano, R. Ruiz-García and E. Pardo, *Inorg. Chim. Acta*, **2008**, 361, 3432–3445.
- 14.- M. Llunell, M.; D. Casanova.; J. Cirera.; P. Alemany; S. Alvarez,SHAPE, version 2.0; Universitat de Barcelona: Barcelona, Spain, 2010.
- 15.- N. F. Chilton.; R. P. Anderson; L. D. Turner; A. Soncini; K. S. Murray, *J. Comput. Chem.***2013**, 34, 1164–1175.
- 16.- a) J. A. Duncan, *J. Am. Chem. Soc.* **2009**, 131, 2416–2416; b) F. Aquilante, L. De Vico, N. Ferre, G. Ghigo, P. A. Malmqvist, P. Neogady, T. B. Pedersen, M. Pitonak, M. Reiher, B. O. Roos, L. Serrano-Andres, M. Urban, V. Veryazov, R. Lindh, *J.*

- Comput. Chem.* 2010, **31**, 224–247; c) V. Veryazov, P. O. Widmark, L. SerranoAndres, R. Lindh, B. O. Roos, *Int. J. Quantum Chem.* **2004**, 100, 626–635; d) G. Karlstrom, R. Lindh, P. A. Malmqvist, B. O. Roos, U. Ryde, V. Veryazov, P. O. Widmark, M. Cossi, B. Schimmelpfennig, P. Neogrady, L. Seijo, *Comput. Mater. Sci.* **2003**, 28, 222–239.
- 17.- A. Arauzo, A. Lazarescu, S. Shova, E. Bartolomé, R. Cases, J. Luzón, J. Bartolomé, C. Turta, *Dalton Trans.* **2014**, 45, 12342. (c) H. X. Zhang, S. Y. Lin, S. F. Xue, C. Wang and J. K. Tang, *Dalton Trans.*, **2015**, 44, 4648.
- 18.- A. Abragam and B. Bleaney, *Electron Paramagnetic Resonance of Transition Ions*, Clarendon Press. Oxford, 1970.
- 19.- a) A. Singh and K. N. Shrivastava, *Phys. Status Solidi B*, **1979**, 95, 273-277 b) K. N. Shrivastava, *Phys. Status Solidi B*, **1983**, 117, 437–458.
- 20.- (a) F. Habib; I. Korobkov; M. Murugesu, *M. Dalton Trans.* **2015**, 44, 6368–6373. (b) Z.-B. Hu, Z.-Y. Jing, M.-M. Li, L. Yin, Y.-D. Gao, F. Yu, T.-P. Hu, Z. Wang, Y. Song, *Inorg. Chem.* 2018, 57, 10761-10767. (c) J. Li, Y. Han, F. Cao, R. M. Wei, Y. Q. Zhang, Y. Song. *Dalton Trans.* **2016**, 45(22), (d) 9279-84. I. Potočák, K. Ráčová, E. ěižmár, L. Váhovská, O. Bukrynov, S. Vitushkina, L. Findoráková, *Polyhedron*, **2017**, 137, 112-121.
- 21.- A. Lunghi, F. Totti, R. Sessoli, S. Sanvit, *Nature Communications*, **2017**, 8, 14620.
- 22.- A. Lunghi, F. Totti, S. Sanvit, R. Sessoli, *Chem. Sci.*, **2017**, 8, 6051–6059.
- 23.- E. Colacio; J. Ruiz; A. Mota; M. A. Palacios; E. Cremades; E. Ruiz; F. J. White; E. K. Brechin, *Inorg. Chem.* **2012**, 51, 5857-5868.
- 24.- A. K. Hassan.; L. A. Pardi; J. Krzystek; A. Sienkiewicz; P. Goy; M. Rohrer; L. C. Brunel, *J. Magn. Reson.* **2000**, 142, 300.
- 25.- APEX2; Bruker AXS: Madison, WI, 2010.
- 26.- SAINT, Version 8.30a; Bruker AXS: Madison, WI, 2013.

- 27.-Sheldrick, G. M. SADABS, Version 2004/1; Bruker AXS:Madison, WI, 2008.
- 28.-G. M. Sheldrick, SHELXL-97, A Program for Crystal Structure Refinement.University of Göttingen, Germany, 1997. SHELXTL Version 2014/7.
<http://shelx.uni-ac.gwdg.de/SHELX/index.php>.
- 29.- L. F. Chibotaru, L. Ungur, *L. J. Chem. Phys.* **2012**, 137, 064112.
- 30.- (a) B. O.Roos,;V.Veryazov;P. O.;Widmark, *Theor. Chim. Acta.*, **2004**, 111, 345;
(b) B. O.Roos,; R. Lindh; P. A. Malmqvist; V. Veryazov; P. O. Widmark, Main Group Atoms and Dimers Studied with a New Relativistic ANO Basis Set.*J. Phys. Chem. A*,**2004**, 108, 2851-2858; (c) B. O.Roos,; R. Lindhn ; P. A. Malmqvist ; V. Veryazov ; P. O. Widmark; New Relativistic ANO Basis Sets for Transition Metal Atoms. *J. Phys. Chem. A*,**2005**, 109, 6575-6579; (d) B. O.Roos,; R. Lindh; P. A. Malmqvist; V. Veryazov; P. O. Widmark, New relativistic ANO basis sets for actinide atoms.*Chem. Phys. Letters*,**2005**, 409, 295-299.

Supplementary Material

Dinuclear vs Tetranuclear CoIIYIII complexes: The effect of increasing molecular size on the relaxation dynamics.

Alberto Masegosa, M. Palacios, Eliseo Ruiz, Silvia Gómez-Coca, J. Krzystek, José. M. Moreno, Enrique Colacio

Table S1.- Continuous Shape Measures calculation for the CoN_3O_3 coordination polyhedron of **1**.

S H A P E v2.1 Continuous Shape Measures calculation
(c) 2013 Electronic Structure Group, Universitat de Barcelona
Contact: llunell@ub.edu

JPPY-6 5 C5v Johnson pentagonal pyramid J2
TPR-6 4 D3h Trigonal prism
OC-6 3 Oh Octahedron
PPY-6 2 C5v Pentagonal pyramid
HP-6 1 D6h Hexagon

Structure [ML6]	JPPY-6	TPR-6	OC-6	PPY-6	HP-6
,	25.478,	11.801,	1.444,	22.035,	30.762

Table S2. Crystallographic data for $[\{\text{Co}(\mu\text{-L})\text{Y}(\text{NO}_3)\}_2(\mu\text{-CO}_3)_2] \cdot 2\text{CH}_3\text{OH} \cdot 2\text{H}_2\text{O}$ (**1**).

Formula	$\text{C}_{54}\text{H}_{86}\text{N}_8\text{O}_{24}\text{Co}_2\text{Y}_2$
Mw	1526.98
Crystal system	Monoclinic
Space group (no.)	P21/n (14)
a (Å)	12.959(3)
b (Å)	12.394(3)
c (Å)	19.345(4)
α (°)	90.000(3)
β (°)	94.40(3)
γ (°)	90.000(3)
V (Å ³)	3097.9(11)
Z	2
Dc (g cm ⁻³)	1.637
$\mu(\text{MoK}\alpha)$ (mm ⁻¹)	2.468
T (K)	100(2)
Observed reflections ^a	6376 (5534)
Rint	0.0536 (0.0290)

Parameters	429
GOF	1.119
R1 ^b	0.0407 (0.0298)
wR ^{2c}	0.0741 (0.0687)
Largest peak and hole (e Å ⁻³)	0.427 and -0.783
^a Values in parentheses for reflections with $I > 2\sigma(I)$.	
^b $R1 = \sum F_o - F_c / \sum F_o $.	
^c $wR2 = \{\sum[w(F_o^2 - F_c^2)^2] / \sum[w(F_o^2)^2]\}^{1/2}$.	

Table S3. Selected distances and angles for $[\{Co(\mu-L)Y(NO_3)\}_2(\mu-CO_3)_2] \cdot 2CH_3OH \cdot 2H_2O$ (**1**).

Bond	amstrongs	Bond/distance	amstrongs
Co2- N1	2.182(2)	Y1-O5	2.3605(17)
Co2-N2	2.199(2)	Y1-O5 (I)	2.3533(17)
Co2-N3	2.250(2)	Y1-O7	2.3884(17)
Co2-O2	2.1541(17)	Y1-O9	2.5821(18)
Co2-O3	2.0996(18)	Y1-O10	2.4611(18)
Co2-O6	2.0706(17)	Y1...Co2	3.4872(7)
Y1-N7	2.955(2)	Co2...Co2 (I)	8.278(2)
Y1-O2	2.2939(17)	Y1...Y1 (I)	3.9987(10)
Y1-O3	2.2833(16)	Co2...Co2 (II)	8.290(2)
Y1-O4	2.5332(19)	Co2...Co2 (III)	8.4321(15)
I= 1-x, 1-y, -z; II= -x, 1-y, -z; III= 1/2-x, -1/2+y, 1/2-z or 1/2-x, 1/2+y, 1/2-z			
Angle	degrees	Angle	degrees
N1-Co2-N2	80.44(8)	O3-Co2-N3	90.18(7)
N1-Co2-N3	102.10(8)	O3-Co2-O2	77.37(7)
N2-Co2-N3	80.42(8)	O6-Co2-N1	96.19(8)
O2-Co2-N1	90.04(7)	O6-Co2-N2	167.60(7)
O2-Co2-N2	98.19(7)	O6-Co2-N3	88.70(7)
O2-Co2-N3	167.31(7)	O6-Co2-O2	93.72(7)
O3-Co2-N1	166.26(7)	O6-Co2-O3	90.17(7)
O3-Co2-N2	95.77(8)		

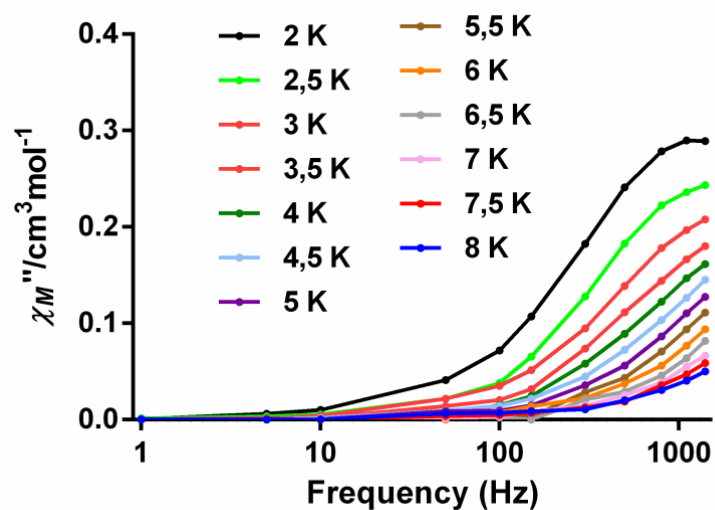


Figure S1.- Frequency dependence of the out-of-phase ac susceptibility for **1** under a magnetic field of 0.025 T at different temperatures.

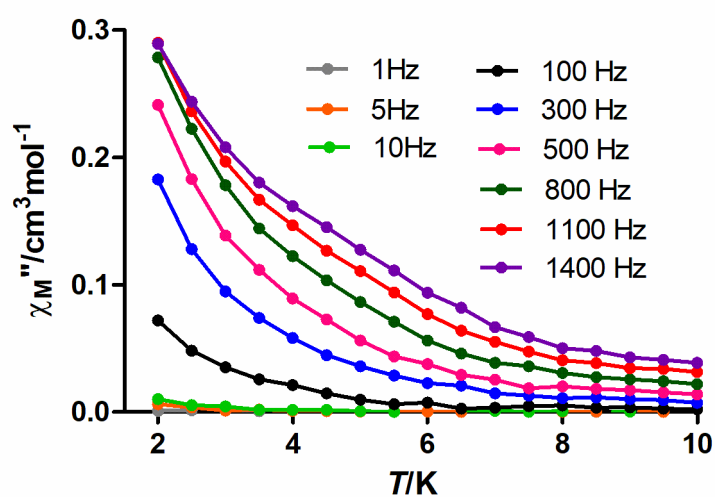


Figure S2.- Temperature dependence of the out-of-phase ac susceptibility for **1** under a magnetic field of 0.025 T at different frequencies.

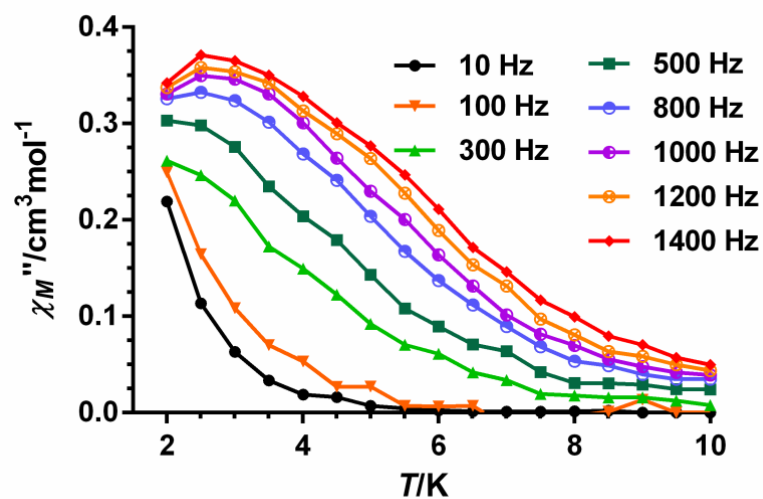


Figure S3.- Temperature dependence of the out-of-phase ac susceptibility for **1** under a magnetic field of 0.25 T at different frequencies.

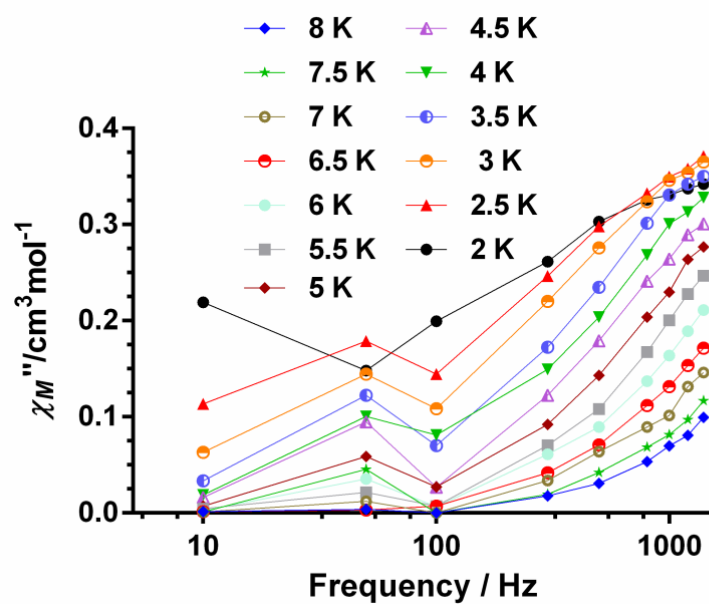


Figure S4.- Frequency dependence of the out-of-phase ac susceptibility for **1** under a magnetic field of 0.25 T at different temperatures

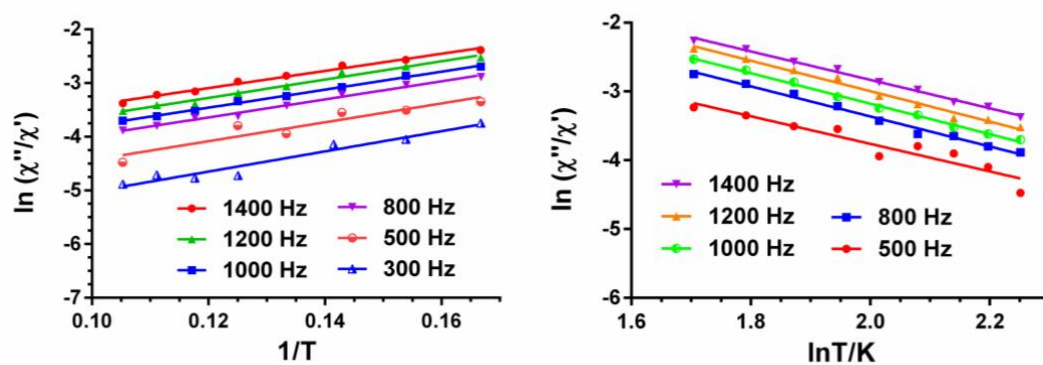


Figure S5.- Temperature dependence of the ratio of the in-phase and out-of-phase *ac* components at different frequencies under a magnetic field of 0.25 T for **1**. Solid lines correspond to the fit of the experimental data to equation 4 (left) and equation 5 (right).

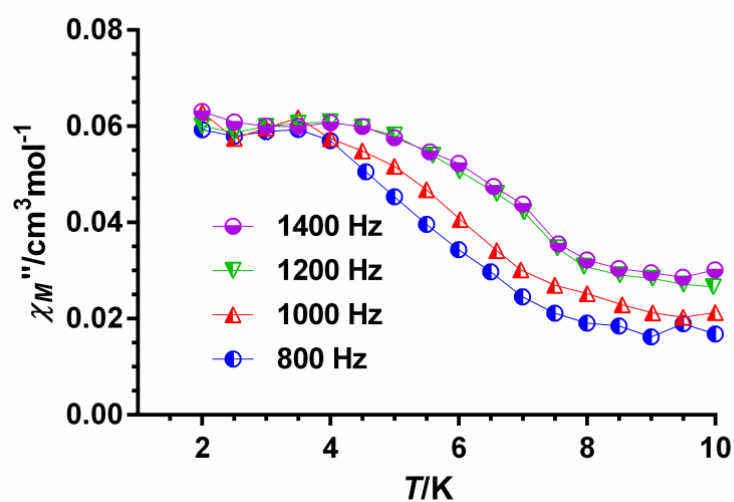


Figure S6.- Temperature dependence of the out-of-phase *ac* susceptibility for **1'** under a magnetic field of 0.25 T at different frequencies.

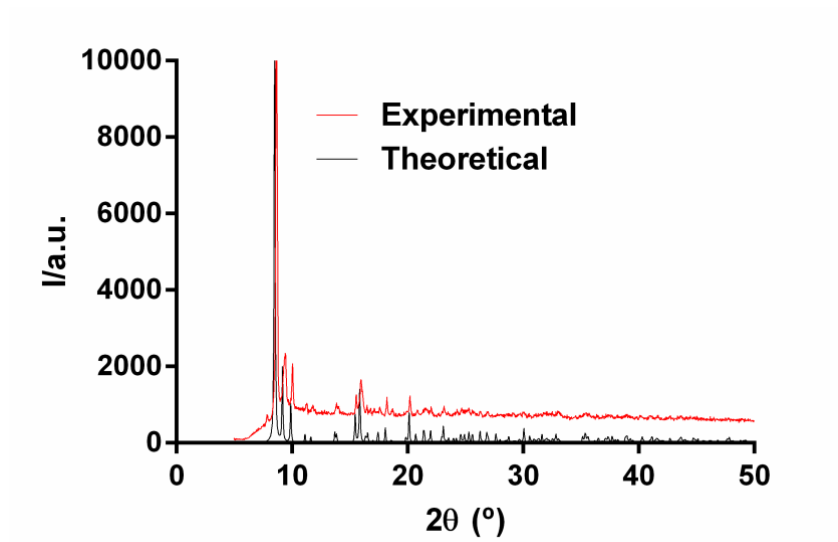


Figure S7 .- Experimental and calculated Powder X-Ray diffraction diagrams for **1'**.